Published in final edited form as:
J Mol Biol. 2007 February 16; 366(2): 687–701.

Magnesium-Cationic Dummy Atom Molecules Enhance Representation of DNA Polymerase β in Molecular Dynamics Simulations: Improved Accuracy in Studies of Structural Features and Mutational Effects

Peter Oelschlaeger[1,*], **Marco Klahn**[1], **William A. Beard**[2], **Samuel H. Wilson**[2], and **Arieh Warshel**[1,*]

1 *University of Southern California, Department of Chemistry, Los Angeles, California*

2 *Laboratory of Structural Biology, National Institute of Environmental Health Sciences, National Institutes of Health, Research Triangle Park, North Carolina*

Summary

Human DNA polymerase β (pol β) fills gaps in DNA as part of base excision DNA repair. Due to its small size it is a convenient model enzyme for other DNA polymerases. Its active site contains two Mg^{2+} ions, of which one binds an incoming dNTP and one catalyzes its condensation with the DNA primer strand. Simulating such binuclear metalloenzymes accurately but computationally efficiently is a challenging task. Here, we present a magnesium-cationic dummy atom approach that can easily be implemented in molecular mechanical force fields such as the ENZYMIX or the AMBER force fields. All properties investigated in this paper, that is, structure and energetics of both Michaelis complexes and transition state (TS) complexes were represented more accurately using the magnesium-cationic dummy atom model than using the traditional one-atom representation for Mg^{2+} ions. The improved agreement between calculated free energies of binding of TS models to different pol β variants and the experimentally determined activation free energies indicates that this model will be useful in studying mutational effects on catalytic efficiency and fidelity of DNA polymerases. The model should also have broad applicability to the modeling of other magnesium-containing proteins.

Keywords

Metalloenzyme; DNA polymerase; molecular dynamics; magnesium ion; mutation

Introduction

All cells rely on DNA polymerases to replicate their DNA molecules[1] and repair them if they have been damaged.[2] These enzymes catalyze the incorporation of nucleotides into a DNA molecule.[3,4] In the case of DNA replication, the DNA molecule is synthesized from a single

*Corresponding authors: Peter Oelschlaeger, University of Southern California, Department of Chemistry, SGM 418, 3620, McClintock Ave., Los Angeles, CA 90089-1062, Phone: (213) 740 7671, Fax: (213) 740 2701, E-mail: poelschl@usc.edu., Arieh Warshel, University of Southern California, Department of Chemistry, SGM 418, 3620, McClintock Ave., Los Angeles, CA 90089-1062, Phone: (213) 740 4114, Fax: (213) 740 2701, E-mail: warshel@usc.edu.

strand DNA template, to which a primer strand is annealed, thus forming a partial DNA double strand (duplex). In the case of DNA repair, DNA polymerases fill up single-stranded gaps resulting from excision of the damaged strand. Prior to the incorporation reaction, a deoxynucleoside triphosphate (dNTP) is bound opposite the template nucleotide and downstream of the 3′-terminal primer nucleotide. After deprotonation, O3′ attacks the dNTP α-phosphorous (αP) and yields a transition state (TS) with a pentacoordinate phosphorous. Ultimately, elimination of pyrophosphate yields the primer product extended by one nucleotide. Mammalian DNA polymerase β (pol β) fills in single-nucleotide gaps as part of base excision repair and represents a popular model enzyme due to its small size.[4–6] It employs two bivalent magnesium ions.[4,7–9] The dNTP-binding Mg^{2+} [Mg(b)] binds the triphosphate of the incoming dNTP, thus positioning it for productive incorporation. Probably, this Mg^{2+} ion also plays a key role in catalysis by stabilizing the leaving group.[10] The catalytic Mg^{2+} [Mg(c)] catalyzes the reaction by both stabilizing the O3′ nucleophile and stabilizing the pentacoordinate TS. A recent high-resolution crystal structure (PDB accession code 2FMS[9]) of human pol β reveals that both Mg^{2+} ions are coordinated octahedrally: Mg(b) by nonbridging oxygens of the α-, β-, and γ-phosphates of the dNTP and by side-chain oxygens of Asp190 and Asp192, and a water molecule; Mg(c) by a nonbridging oxygen of the dNTP α-phosphate (serving as a bridging ligand between the two Mg^{2+} ions), the primer O3′, the other two side-chain oxygens of Asp190 and Asp192, a side-chain oxygen of Asp256, and a water molecule (Figure 1A). In a previous crystal structure of pol β, (PDB accession code 1BPY[8]), the metal ion in the Mg(c) binding site was coordinated tetrahedrally with unusually large metal-ligand distances for a Mg^{2+} ion. A new high-resolution structure (PDB accession code 2FMQ[9]), in which Mg(c) is replaced by a Na^{+} [Na(c)] (Figure 1B), exhibits the same coordination geometry, suggesting that in the 1BPY structure the metal ion in the catalytic site was Na^{+} rather than Mg^{2+}.[4,9]

Computer simulations can help elucidate certain aspects of the function of DNA polymerases such as the effect of mutations on conformational changes[11,12] or energetics.[13–16] Magnesium ions are usually represented as ions with a formal point charge of +2 that interact with the protein environment and the substrate through nonbonded interactions. In binuclear sites as in pol β, however, high charges can lead to instabilities, resulting in an alteration of the proper coordination of the Mg^{2+} ions by the ligands and repulsion between the two Mg^{2+} ions. Although such artifacts can be avoided by imposing positional restraints on the Mg^{2+} ions or restraining the distances between the Mg^{2+} ions and their ligands, it is desirable to find solutions to represent the Mg^{2+} ions without using restraints. The combination of quantum mechanical and molecular mechanical (QM/MM) approaches (for a review see Ref.17) presents such a solution, however, at computational cost. In addition, instructive work has been done on the optimization of van der Waals (vdW) parameters of metal ions used in molecular mechanical (MM) force fields.[18–20] The goal of this study is to find a computationally efficient and accurate solution that can be easily implemented in different force fields such as the AMBER[21] or the polarizable ENZYMIX[22] force fields used in the MOLARIS program suite.[22,23] The focus will be placed on the Åqvist-Warshel (AW) model[24] that uses cationic dummy atoms and has proven very useful in accurately representing the energetics and structures of systems with transition metals such as octahedrally coordinated bivalent manganese ions[24] and tetrahedrally coordinated bivalent zinc ions in mononuclear[25–27] and binuclear[28–30] metalloenzymes. The underlying idea of this approach is to represent the partially covalent and partially electrostatic nature of the coordinative bond by locally splitting up the space between the transition metal atom and the ligand into a covalent bond (between the metal atom and a cationic dummy atom) and an electrostatic interaction (between the cationic dummy atom and the partially negatively charged ligand). Such models allow for stable coordination geometry by placing the cationic dummy atoms at the defined positions around the central metal atom and for a smaller repulsion between the metal ions in binuclear sites by distributing the positive charge over the cationic dummy atoms.

Here we test if such a treatment is suitable for the octahedrally coordinated bivalent earth alkali magnesium ions in the binuclear active site of pol β. Our magnesium-cationic dummy atom model (MD_6^{2+}) is validated using the recent high-resolution crystal structures of human pol β[9] with either two Mg^{2+} ions (MgMg structure, PDB accession code 2FMS) or a Mg^{2+} ion in the dNTP binding site and a Na^+ ion in the catalytic site (MgNa structure, PDB accession code 2FMQ) as a benchmark. The MD_6^{2+} model is compared to models with standard ENZYMIX and AMBER one-atom representations for the Mg^{2+} ions as well as to the one-atom Mg^{2+} ion used in our previous studies.[14,16] Using the MD_6^{2+} model, both crystal structures are modeled more accurately. Furthermore, the MD_6^{2+} model's potential to reproduce catalytic efficiencies from experiment[6] is tested by calculating binding free energies of TS models of different dNTPs to different pol β variants using the all-atom LRA method.[31,32] The success of these simulations promises that the MD_6^{2+} model will be a useful element for future theoretical studies on the function and fidelity of DNA polymerases.

Results

Structures of pol β-DNA-dTTP ternary complexes

Several van der Waals values for bivalent traditional one-atom magnesium ions were tested in combination with the nonpolarizable or polarizable ENZYMIX force field or the AMBER force field. Using these different constellations in MD simulations of two crystal structures[9] of human pol β, one exhibiting two magnesium ions (MgMg structure, Figure 1A) and one exhibiting a magnesium ion and a sodium ion (MgNa structure, Figure 1B) in the binuclear active site, the crystal structures were best reproduced with the Mg^{2+} ions used in our previous studies (vdW radius R^* = 1.300 Å, well depth ε = 0.06).[15,16] The performance of these Mg^{2+} ions will be examined in more detail and compared to the MD_6^{2+} model below. All other traditional one-atom Mg^{2+} ions were not able to maintain both the MgMg and MgNa structures. Using the standard AMBER Mg^{2+} ions (R^* = 0.7926 Å, ε = 0.8947)[18] within the AMBER force field, the coordination of both Mg(b) and Mg(c) in the MgMg structure changed: Mg(b) lost contact to its ligands Asp192 and O2B (a nonbridging β-phosphate oxygen of the dNTP) and was instead coordinated by O3B (the oxygen bridging the β- and γ-phosphates of the dNTP); Mg(c) lost contact to its ligands O3′ of the primer and O1A (a nonbridging α-phosphate oxygen of the dNTP coordinating both metal ions in the crystal structure[9]). In the MgNa structure with Na(c) being represented as the standard AMBER Na^+ ion (R^* = 1.868 Å, ε = 0.00277),[18] Mg(b) lost contact to O3G of the dNTP and a water molecule, while Na(c) was coordinated by both side-chain oxygens of Asp256 instead of only one as in the crystal structure.[9] The MgMg structure was modeled quite accurately when using the standard ENZYMIX Mg^{2+} ions (R^* = 0.735 Å, ε = 50.567) in combination with the nonpolarizable ENZYMIX force field and even more accurately when using the polarizable ENZYMIX force field. However, the MgNa structure, in which Na(c) was represented by the standard ENZYMIX Na^+ ion (R^* = 1.745 Å, ε = 0.00444), was not maintained: Na(c) lost contact to O1A but was additionally coordinated by two water molecules, giving rise to five-fold coordination as opposed to the four-fold coordination observed in the crystal structure.[9] With the polarizable force field, the deviations from the crystal structure were smaller than with the nonpolarizable force field, but still significant.

Even though using Mg^{2+} ions with R^* = 1.300 Å and ε = 0.06[15,16] yielded the best structural results among the traditional one-atom Mg^{2+} models, there were some significant discrepancies between the crystal structures and the modeled structures, i.e., increased Mg(b)-Mg(c), Mg(b)-Na(c), and O1A-Mg(b) distances. In order to overcome these deviations in modeled pol β structures without using restraints, we developed a new model for bivalent magnesium ions. In this model, the magnesium ion is represented by a central atom (M) positioned at the crystallographic position of the metal ion and six cationic dummy atoms (D) that are positioned

octahedrally around and covalently connected to M (Table 1) and interact with the ligands through nonbonded interactions. Using the resulting MD_6^{2+} model in adiabatic charging free energy perturbation (FEP) calculations, the density function theory (DFT) calculated and experimentally observed solvation free energy could be reproduced (Table 2). Furthermore, the structural and energetic behavior of this model in small model complexes (Figure 2) in the gas phase and in solution was tested with the ENZYMIX and AMBER force fields and corresponded well with data from DFT calculations and X-ray crystallography (Tables 3 and 4). Overall, the MD_6^{2+} model was successfully employed with all tested force fields. Using the polarizable ENZYMIX force field gave more accurate results than using the nonpolarizable version; however, also the computationally more efficient nonpolarizable force fields gave accurate results within the confines of molecular mechanics force fields.

The MD_6^{2+} model was then tested in MD simulations of the MgMg and MgNa structures of pol β using either the AMBER force field or the ENZYMIX force field in its nonpolarizable and polarizable forms for the protein and DNA residues. Using this approach, the crystal structures were reproduced more accurately than when using the traditional one-atom representation for the Mg^{2+} ions. This is demonstrated exemplarily with the AMBER force field by critically analyzing the ability of the traditional one-atom Mg^{2+} ions with $R^* = 1.300$ Å and $\varepsilon = 0.06$[15,16] and the MD_6^{2+} model to accurately reproduce the two crystal structures[9] in unconstrained MD simulations over 1 ns at different temperatures (100 K, 200 K, and 300 K). Three critical distances were measured in 200 configurations collected over the course of each simulation: the distance between the two magnesium ions, the distance between Mg(b) and O1A, and the distance between Mg(b) and O2B. The progressions of these distances in both models over time are shown in Figure 3 for the MgMg structure and in Figure 4 for the MgNa structure. The average values ± standard deviations are reported in comparison to the corresponding distances in the X-ray crystal structures in Table 5. The distances between the other ligands and the metal ions were in agreement with experimental values (Table 4) and are not reported.

In simulations of the MgMg structure, the average Mg(b)-Mg(c) distance increased compared to the crystal structure in both approaches, however much more significantly in the MgMg (two traditional one-atom Mg^{2+} ions) model (by 0.38–0.46 Å or 12–13%) than in the MD_6MD_6 (two MD_6^{2+} molecules) model (no more than 0.3 Å or 9%) (Figure 3, panels A, D, and G). For the average Mg(b)-O1A distance, the discrepancy between the two models was even more pronounced: this distance was increased by 0.28–0.37 Å or 14–18% in the MgMg model compared to less than 0.15 Å or 7% in the MD_6MD_6 model (Figure 3, panels B, E, and H). The average Mg(b)-O2B distance was in fair agreement with the crystallographic distance in both models: it was slightly increased by no more than 0.13 Å or 7% in the MgMg model and by no more than 0.1 Å or 5% in the MD_6MD_6 model (Figure 3, panels C, F, and I). In all cases, the standard deviations, an indicator for the fluctuation of the measured distances around the average value, were larger in the MgMg model than in the MD_6MD_6 model. Overall, the MD_6MD_6 model represents the MgMg crystal structure more accurately. Only the Mg(b)-Mg(c) distance increased noticeably by up to 9%. All the magnesium-triphosphate oxygen distances were between 2.13 and 2.20 Å and therefore in excellent agreement with the experimentally observed distances (Table 4). In contrast, in the MgMg model both the Mg(b)-Mg(c) distance and the Mg(b)-O1A distance deviated significantly from the crystal structure by up to 13% and 18%, respectively. These distances are likely correlated, because O1A as a bridging ligand keeps the Mg(b)-Mg(c) distance short. Their correlation can be observed in Figure 3: at 100 K, both distances increase after 850 ps (panels A and B); at 200 K, both distances decrease between 900 and 950 K (panels D and E); at 300 K, both distances peak at, e.g., 20 ps, 405 ps, and 635 ps (panels G and H).

We also analyzed the position of the primer 3′ hydroxyl relative to αP in the Michaelis complex of the MgMg structure simulated at 300 K with both approaches. The position of this residue might give insights into the subsequent nucleophilic attack of the deprotonated O3′ on αP. In the crystal structure, the O3′-αP distance is 3.40 Å and the angle O3′-αP-N3A (bridging nitrogen between αP and β P) is 160°.[9] In the MgMg model simulated at 300 K, the O3′-αP distance was 3.32 ± 0.14 Å and the O3′-αP-O3A angle was 169 ± 5°, in good agreement with the X-ray crystal structure. In the MD_6MD_6 model simulated at 300 K, these values were 3.18 ± 0.09 and 170 ± 4°, deviating a little more from the crystal structure.

In simulations of the MgNa structure, the average Mg(b)-Na(c) distance increased compared to the crystal structure in both approaches. In contrast to the MgMg structure, the increase in both models was comparable at 100 K and 200 K. In the MgNa model, the average distance increased by 0.05–0.22 Å or 1–7%; in the MD_6Na model, it increased by 0.03–0.26 Å or 1–8%. However, at 300 K, the Mg(b)-Na(c) distance was noticeably increased in the MgNa model (by 0.38 Å or 11%), whereas it was increased only by 0.23 Å or 7% in the MD_6Na model. The Mg(b)-O1A distance was acceptable in both models, slightly above 2.2 Å in the MgNa model and slightly below 2.2 Å in the MD_6Na model. Similarly, the Mg(b)-O2B distance was around 2.2 Å in the MgNa model and around 2.15 Å in the MD_6Na model and therefore in good agreement with the crystal structure in both models. In all cases, the standard deviations were equal or larger in the MgNa model than in the MD_6Na model. Overall, using the MD_6^{2+} model, the MgNa crystal structure could be reproduced with higher fidelity than with a traditional one-atom Mg^{2+} ion; however, the deviations in the MgNa model are moderate compared to the MgMg model.

We tested both approaches, the regular Mg^{2+} ions and the MD_6^{2+} model, for their potential to restore the geometry of the MgMg structure by starting from the MgNa structure and replacing the Na^+ ion in the catalytic metal binding site by the two magnesium models. In the following, these two models will be referred to as MgNa->MgMg and MgNa->MD_6MD_6, respectively. The conformation of the 3′-terminal sugar of the primer had to be changed from 2′-endo to 3′-endo[4] in order to allow coordination of O3′ to Mg(c). Within a few ps of simlation at 300 K, octahedral coordination of Mg(c) as opposed to distorted tetrahedral coodination in the starting structure was restored in both models and maintained during prolonged 1.1 ns of simulation at this temperature. In the MgNa->MgMg model, O3′ and a water molecule had joined the three side-chain oxygens of Asp190, Asp192, and Asp256 and O1A of the dTTP as Mg(c) ligands. The Mg(b)-Mg(c) distance and the Mg(b)-O1A distance were relatively high with 3.88 and 2.40 Å, respectively, and very similar to the simulated MgMg model started from the MgMg structure (Table 5A). In the MgNa->MD_6MD_6 model, O3′ and the second side-chain oxygen of Asp190 completed octahedral coordination of Mg(c), with Asp190 now serving as a bidentate ligand for Mg(c) and one of its side-chain oxygens as a bridging ligand for both magnesium ions, thus keeping the Mg(b)-Mg(c) distance low at 3.26 Å. In the MgNa->MgMg model, the O3′-αP distance was 3.24 Å and the O3′-αP-O3A angle was 165°; in the MgNa->MD_6MD_6 model, the respective values were 3.10 Å and 164°, compared to 3.4 Å and 160° in the crystal structure. Thus, although both structures deviated slightly from the MgMg crystal structure,[9] they both restored the main features of the pre-TS structure: octahedral coordination of both magnesium ions and proper orientation of the primer O3′ for nucleophilic attack on αP of the dNTP.

In summary, the main advantage of the MD_6^{2+} model over the Mg^{2+} model, especially in the MgMg structure, is that we can reproduce the crystal structure accurately without having to apply positional restraints on the Mg^{2+} ions or distance restraints between the Mg^{2+} ions and their ligands. This should also facilitate the determination of binding free energies of dNTP substrates and TS models to pol β. The performance of both models in such calculations will be examined in the next sections.

Structural comparison of modeled Michaelis and TS complexes

Prior to the all-atom LRA calculations, the Michaelis and TS complexes were equilibrated at 30 K and then simulated at 310 K for 100 ps. Some structural features deviated significantly between the resulting Michaelis and TS complexes apart from the artificially imposed restraints in the TS complexes (shortened O3′-αP distance and extended αP-O3A distance), most notably the distance between O3A and Mg(b). In the crystal structure, the N3A-Mg(b) distance is 3.25 Å. Since it is hard to directly compare N3A (the (α, β)-phosphate bridging imido nitrogen in the crystal structure[9]) to O3A (the bridging oxygen modeled at this position), we also want to mention that the O3A-Mg(b) distance in the 1BPY crystal structure,[8] which is more comparable to our model, is 3.38 Å. In the simulated Michaelis complex of the WT bound to dTTP, this distance was 3.11 Å and 3.05 Å, using the Mg^{2+} model and the MD_6^{2+} model, respectively, slightly smaller than in the crystal structures. In the simulated WT-TS complex, this distance was significantly decreased to 2.55 Å and 2.62 Å, using the Mg^{2+} model and the MD_6^{2+} model, respectively.

Determination of binding free energies of dNTPs and TS models to pol β variants

Previously, we have investigated the effects of mutations on catalytic efficiencies of pol β using traditional one-atom Mg^{2+} ions, the positions of which were restrained with 10 kcal/(mol*Å2) to correct for possible force field deficiency.[16] Although we obtained good agreement between our calculations and the experimental data, the observed correlation was qualitative rather than quantitative. Furthermore, since we used data from different experimental studies that were carried out under slightly different conditions, it was hard to assign the cause for outliers to either the computational or experimental procedures. Here, we only investigate pol β variants that were measured experimentally under the same conditions in the same laboratory,[6] assuming that this provides a self-consistent data set. The investigated mutations are all in proximity to the incoming nucleotide or nascent base pair (Figure 1A) and have a significant effect on catalytic efficiency (Table 6). Arg149 is at a distance of 4.6 Å from the γ-phosphate of the incoming dNTP. The R149A mutation increases K_d about 6.5-fold compared to wild type, resulting in 6- to 7-fold decrease in k_{pol}/K_d for incorporation of dTTP opposite A (A:T) and dCTP opposite G (G:C). Arg183 is at a distance of 3.0 Å from the β-phosphate. For A:T, the R183A mutation increases K_d about 4-fold and decreases k_{pol}/K_d about 100-fold. For G:C, this mutation increases K_d about 3-fold, but decreases k_{pol}/K_d only 15-fold. Lys280 is at a distance of 3.4 Å from the template base. The K280A mutation increases K_d for G:C about 3-fold while not affecting k_{pol}, leading to about a 3-fold decrease in k_{pol}/K_d. The deduced differences in ΔG_{bind} are within 2 kcal/mol and the differences in $\Delta g^{\ddagger}_{enz}$ are within 3 kcal/mol. Since these residues are in the active site, they are likely to affect dNTP binding and catalysis rather than conformational rearrangements, which would be hard to capture in the time scale of our simulations.

We computed the free energies of binding of either dTTP opposite template A (A:T) or dCTP opposite template G (G:C) in the different pol β variants using the MgMg model and the MD_6MD_6 model in all-atom linear response approximation (LRA) calculations and plotted the experimentally determined values $\Delta G_{bind,\ exp}$. versus the calculated values $\Delta G_{bind,\ calc}$.. With the MgMg model, we were able to reproduce the experimental trend, however, with a poor correlation (R2 = 0.44, Figure 5A). Using the MD_6MD_6 model, a better correlation was obtained (R2 = 0.70, Figure 5B).

We then computed the free energies of binding of the TS models dTTP-TS and dCTP-TS opposite A and G, respectively, to the different pol β variants using both models. With the MgMg model, we obtained a reasonable correlation between the experimentally determined binding free energies of the TS $\Delta g^{\ddagger}_{enz,\ exp}$ and the calculated values $\Delta g^{\ddagger}_{enz.\ calc.}$ (R2 = 0.75,

Figure 6A). Using the MD_6MD_6 model, an excellent correlation was obtained (R2 = 0.95, Figure 6B).

In all cases (Figures 5 and 6), there was no obvious separation between the values for A:T and those for G:C, indicating that the parameterization and the partial electrostatic charges used in our calculations give a good representation of both incoming dNTPs. Note that the absolute computed values for the binding free energies are of a different magnitude than the experimental values. This can be attributed mainly to the fact that we have not used a dielectric constant in our all-atom representation of the molecular systems (see detailed discussion in Ref.16). When we divide the computed values by the experimental values, for instance, for the Michaelis complexes, we obtain an effective dielectric constant of 35 for the MgMg model and 40 for the MD_6MD_6 model, values in the range of the effective dielectric constants usually used to calculate charge-charge interactions in proteins.[33]

Discussion

Structural model with improved accuracy

The use of magnesium-cationic dummy atom molecules (MD_6^{2+}) rather than traditional one-atom representation for Mg^{2+} ions follows up on the early AW model[24] and subsequent studies.[25–28] It combines the benefits of nonbonded interactions in reproducing solvation free energies and in keeping the metal site flexible with the benefits of covalent bonds, such as stable coordination geometry. Attaching cationic dummy atoms to the central metal atom at defined positions leads to more directed electrostatic interactions with ligands and delocalization of the charge to prevent repulsion in binuclear sites. As evidenced by our detailed comparison of the structures of Michaelis complexes obtained from MD simulations using both models, the MD_6^{2+} model always performed better. In particular, the Mg(b)-Mg(c) distance and the distance between Mg(b) and O1A of the incoming dNTP were much closer to the X-ray crystallographic distances in the MgMg structure.[9] The MD_6^{2+} model was also superior in reproducing the crystallographic structure of the MgNa structure,[9] although the Mg^{2+} model also performed satisfactorily in this case. We attribute this mainly to the fact that Na^+ has a smaller positive charge than Mg^{2+}, resulting in a smaller repulsion between the active site metals. In the MgMg structure obtained with the Mg^{2+} model, the major deviations from the crystal structure seem to originate from the repulsion of the two metal ions, which also affects the Mg(b)-O1A distance (Figure 3). Apart from that, Mg^{2+} is always coordinated octahedrally with reasonable magnesium-ligand distances. Therefore, the MD_6^{2+} model should be especially effective in modeling binuclear metalloproteins, in which two magnesium ions are at a small distance.

Originally, the idea of using cationic dummy atoms was used to account for charge transfer between ligands and transition metals by moving parts of the positive charge toward the ligands. Here, we report the successful application of this model to the earth alkali metal magnesium. Although it is not a transition metal, it is capable of forming complexes, which involve empty *d*-orbitals. This provides a physical rationale for using cationic dummy atoms in this case. It will be interesting to see whether the MD_6^{2+} model will also be useful in modeling the structure of other binuclear magnesium proteins.

The fact that we could translate the MgNa structure into the MgMg structure with both models suggests that the unexpected coordination of the Mg(c) ion in the previous crystal structure 1BPY[8] was due to a substitution of the magnesium ion by a sodium ion. These two ions cannot be distinguished in X-ray crystal structures because they exhibit the same electron density.[4] In general, MD simulations could be employed more frequently to validate the identity of metal ions in crystal structures.

Small positional restraints were used in the calculations of binding free energies of dNTPs and dNTP-TS models to the enzymes (see Computational Procedures for details). These were not necessary to maintain the positions or coordination of the magnesium ions or the protein but only to maintain the structure of the DNA. That is, the simulations indicated that the DNA structure may not correspond to the most stable configuration of the model used because of the 90º bend and the partially single-stranded DNA. This instability was observed with both the traditional one-atom representation for the magnesium ions and the MD_6^{2+} model. In the Michaelis complexes, which very closely resemble the crystallographic structure, the integrity of the DNA structure could be maintained by applying a very small restraint of 0.03 kcal/(mol*A2). In the TS complexes, where the primer O3′ is connected to Pα of the incoming dNTP, a larger restraint of 0.5 kcal/(mol*A2) was necessary to keep the upstream duplex DNA intact.

Improved energetics

Using the MD_6^{2+} model, we could reproduce experimental kinetic data in computer simulations more accurately than using regular Mg^{2+} ions. For the calculation of binding free energies of dNTP substrates, R^2 improved from 0.44 using the Mg^{2+} model (Figure 5A) to 0.70 using the MD_6^{2+} model (Figure 5B). Previously, we have already experienced that direct calculation of the binding of the TS gives better results and correlations than separate calculations of the binding and catalytic steps.[16] Therefore, we want to focus on the calculation of binding free energies of TS models to different pol β variants to obtain $\Delta g^{\ddagger}_{enz}$, which corresponds to the catalytic efficiency k_{pol}/K_d. With the Mg^{2+} model, we obtained a moderate correlation between experiment and computation (R2 = 0.75, Figure 6A), but the correlation obtained with the MD_6^{2+} model is excellent (R2 = 0.95, Figure 6A) and gives us confidence that we will be able to reproduce and predict the catalytic efficiencies of other mutations. In future studies, we want to extent our procedure to the incorporation of incorrect dNTPs in order to elucidate the molecular mechanisms of DNA polymerase fidelity.

Possible mechanistic implications

It is impossible to obtain a conclusive mechanistic picture without performing an actual simulation of the reaction process (eg. Ref14). However, it might be useful to speculate about some mechanistic features by considering the simulated reactant state and TS. More specifically, the Michaelis complexes simulated with both models resemble the productive pre-TS conformation more than the crystal structure, that is, the distance between the nucleophile O3′ and αP is shorter (3.18 Å in the MD_6MD_6 model and 3.32 Å in the MgMg model compared to 3.40 Å in the crystal structure) and the angle O3′-αP-O3A is closer to 180º (169º in the MD_6MD_6 model and 170º in the MgMg model compared to 160º in the crystal structure). A possible explanation for this observation is that the imido nitrogen N3A in the cocrystallized dUTP analogue has a smaller electronegativity than O3A in dNTP, thus withdrawing less electron density from αP and keeping O3′ farther away from αP. This scenario is in agreement with the fact that no chemistry is observed with the dUTP analogue, while dNTPs are incorporated very rapidly. At any rate, our simulations suggest that O3′ of the primer will be positioned in a very favorable position for nucleophilic attack on αP, and even more so in the MD_6MD_6 model than in the MgMg model.

After nucleophilic attack and formation of the pentacoordinate αP in the TS, pyrophosphate ($P_2O_7^{4-}$) is eliminated and the tetracoordinate αP restored. The distance O3A-αP is extended in the TS to about 2.2 Å[14] and then further extended until the O3A-αP bond breaks. Since the TS resembles the product state to some extent, we can hypothesize on the elimination step and the nature of the product state. In the TS complex modeled with either Mg^{2+} or MD_6^{2+}, O3A moves closer to Mg(b) compared to the Michaelis complex: the O3A-Mg(b) distance in the TS model is 2.6 Å compared to 3.1 Å in the modeled and 3.25 Å in the crystallized Michaelis

complex. Thus, it seems feasible that O3A further approaches Mg(b) as the O3A-αP bond breaks during the elimination step and that the eliminated pyrophosphate coordinates Mg(b) in a tridentate fashion: with the two nonbridging oxygens of the β- and γ-phosphates that already coordinate it in the Michaelis complex plus O3A. The $[Mg(P_2O_7)]^{2-}$ chelate complex generated in this way would be very stable and could leave the active site after the catalytic cycle, as has been proposed previously.[34] This possibility supports the idea that the dNTP-binding magnesium ion could serve as a "shuttle" for import of the dNTP and export of pyrophosphate. Without the magnesium ion, these molecules would be four-fold negatively charged, which would likely inhibit their transfer into and out of the protein.

Concluding Remarks

The magnesium-cationic dummy atom (MD_6^{2+}) model presented here is an effective approach to model pol β using molecular mechanics. Its computational efficiency is comparable to that of regular traditional one-atom Mg^{2+} ions. However, all properties investigated in this paper, that is, structure and mutational effects on energetics of both Michaelis complexes and TS complexes were represented more accurately using the MD_6^{2+} model than using the traditional one-atom representation for Mg^{2+} ions. For small model complexes, the MD_6^{2+} model gave good results using both the nonpolarizable and polarizable ENZYMIX and the AMBER force fields. Likewise, it enabled us to accurately reproduce ternary pol β /DNA/dNTP structures with all tested force fields. We expect that the MD_6^{2+} model can be easily implemented in other commonly used force fields and that it will be useful to study other magnesium-containing proteins. The excellent agreement (R2 = 0.95) between calculated binding free energies of dTTP-TS and dCTP-TS models to different enzyme variants and the corresponding experimentally determined activation free energies suggests that the magnesium-cationic dummy atom model will assist the investigation and prediction of mutational effects on catalytic efficiencies and DNA polymerase fidelity.

Computational Procedures

Refinement of the magnesium-cationic dummy atom model

The Mg^{2+} ions were represented by octahedral molecules (MD_6^{2+}) with covalent bonds between the central magnesium atom (M) and the cationic dummy atoms (D) and between adjacent dummy atoms, following the early AW model[24] and subsequent studies.[25–28] The vdW parameters and the charges were obtained by a systematic refinement which involved the following steps: the vdW coefficients A and B and the charges of M and D were chosen by fitting the simulated solvation free energy of Mg^{2+} in water to the corresponding observed free energy (−454.2 kcal/mol[35]) and by fitting the calculated energy of the $[Mg(H_2O)_6](H_2O)_{12}^{2+}$ complex to the corresponding result of a DFT calculation (−460.8 kcal/mol[36]). This high solvation free energy could be achieved by increasing the charge of the dummy atoms D to +0.5 and by imposing a charge of −1.0 on the central atom M to keep the overall charge of the MD_6^{2+} molecule at +2.0. The calculated solvation free energy of the MD_6^{2+} model was evaluated by an adiabatic charging FEP procedure[37,38] using the POLARIS module of the MOLARIS program suite.[22,23] The corresponding results using the nonpolarizable and polarizable ENZYMIX force field were −456.3 kcal/mol and −456.2 kcal/mol, respectively (Table 2). The vdW coefficients of M were also adjusted to approximate distances and dissociation energies between Mg^{2+} ions and different ligands determined in gas-phase DFT calculations (B3LYP/6-311++G**) carried out with the Gaussian03 program.[39] In addition to the Mg^{2+} ion and the ligand of interest, five water molecules were included to saturate the other coordination positions in these calculations (Figure 2). The results of the DFT calculations and the corresponding gas-phase MM calculations with the MD_6^{2+} molecule of these model complexes using the ENZYMIX[22] and AMBER[21] force fields implemented in the MOLARIS program[23] are reported in Table 3. The ENZYMIX force field was used either in its

nonpolarizable or in its polarizable form. Charges of the ligand molecules in the MM calculations were taken from the ENZYMIX and AMBER libraries (H_2O and CH_3OH) or were calculated at the B3LYP/6-311++G** level using a PCM solvation model[40] implemented in Gaussian03.[39] Furthermore, the relevant distances between ligands and MD_6^{2+} were also determined after minization of these systems in solution. The results are shown in Table 4 and compared to the corresponding distances in high resolution crystal structures of magnesium-containing metalloproteins, where CH_3OH of the model complexes is compared to serine and threonine[41] and PO^{3-} and HPO_4^{2-} are compared to phosphate groups that coordinate to Mg^{2+} through nonbridging oxygens.[9] In our implementation of the AMBER force field in MOLARIS, we have previously changed the vdW radii of nonbridging phosphate oxygens (AMBER atom types O2 and O3) and carboxylate oxygens (AMBER atom type O2) from 1.66 Å to 1.9 Å (O2) and from 1.7 Å to 1.9 Å (O3), because these gave more accurate structures in long MD simulations.[15] We also tested the original AMBER vdW radii, but were not able to reproduce mutational effects as accurately as with our modified vdW radii.

Structures of pol β-DNA-dNTP ternary complexes

The coordinates of the recently published X-ray crystal structures of human pol β[9] were used for this study. The MgMg structure (PDB accession code 2FMS) features two Mg^{2+} ions in the dNTP-binding and the catalytic site [Mg(b) and Mg(c)], while the MgNa structure (PDB accession code 2FMQ) exhibits a Mg^{2+} ion in the dNTP-binding site [Mg(b)] and a Na^+ ion in the catalytic site [Na(c)]. Both structures contain human pol β in the closed conformation bound to a single-gap DNA substrate with a dUTP analog [2′-deoxyuridine-5′(α, β)-imido triphosphate] positioned for incorporation opposite the template adenine. In the dUTP analog, the phosphodiester oxygen bridging αP and β P is replaced by an imido group, which prevents the S_N2 reaction. Therefore, a deoxycytidine could be used at the 3′ terminus of the primer rather than a dideoxycytidine.[4,9] For calculations modeling the Michaelis complex of dTTP bound opposite adenine, the imido group of the dUTP analog was replaced by an oxygen and the uracil base was replaced by thymine (Figure 1). For calculations modeling the Michaelis complex of dCTP opposite guanine, the template adenine was “mutated” to guanine and the incoming dTTP was “mutated” to dCTP. The partial charges of the triphosphate parts of the dNTPs were calculated at the B3LYP/6-31G* level using a PCM solvation model[40] implemented in Gaussian03,[39] and the partial charges of the ribose and bases were adjusted from the AMBER[21] libraries to yield a formal charge of −4.0 for both dTTP and dCTP. The main portion of the negative charge was located on the triphosphate. The other nucleotides of the DNA and the protein residues were represented either by the AMBER[21] or the ENZYMIX[22] amino acid and nucleic acid libraries. Sodium ions were modeled as standard ENZYMIX (R^* = 1.745 Å, ε = 0.00444) or AMBER (R^* = 1.868 Å, ε = 0.00277)[18] Na^+ ions. Magnesium ions were represented either by the standard ENZYMIX (R^* = 0.735 Å, ε = 50.567) or AMBER (R^* = 0.7926 Å, ε = 0.8947)[18] Mg^{2+} ions, as the one used in our previous studies (R^* = 1.300 Å, ε = 0.06),[15,16] or as the MD_6^{2+} molecules described above and in Table 1. In the latter case, the position of M was chosen as the crystallographic position of Mg^{2+} and the positions of the dummy atoms D were chosen between the positions of the Mg^{2+} ions and their ligands, 0.9 Å from the Mg^{2+} ion. The resulting structures including crystal water molecules were immersed in a 20 Å sphere of surface-constrained all-atom solvent (SCAAS)[42] of TIP3P[43] water molecules and a 22 Å sphere of Langevin dipole water molecules, surrounded by a continuum water model.[22] The center of these spheres was positioned at the geometric center of region I (the incoming dNTP). To test whether the MgNa structure could be transferred into the MgMg structure in MD simulations, Na^+ was replaced by Mg^{2+} or MD_6^{2+}, yielding the two models MgNa->MgMg and MgNa->MD_6MD_6. Since no coordination of Mg(c) by O3′ was achieved starting from the 2′-endo conformation of the 3′-terminal primer sugar in the MgNa structure, we changed its conformation to 3′-endo as in the MgMg structure.

Structures of pol β-DNA-dNTP TS complexes

To generate TS models for the incorporation of dCTP and dTTP (dCTP-TS and dTTP-TS), a 1.7 Å bond was added between the deprotonated O3′ of the 3′-terminal primer cytidine and αP of the dNTP; the bond between αP and the (α, β)-phosphodiester oxygen O3A was extended by using a harmonic restraint with a reference distance of 2.2 Å and a force constant of 1,000 kcal/(mol*Å2). In the product state, this bond is cleaved, yielding a pyrophosphate leaving group.[4] The partial charges of dCTP-TS and dTTP-TS were determined in the same fashion as described above for dCTP and dTTP, except that now the dCTP and dTTP had a formal charge of −4.5 and the attacking 3′-terminal primer cytidinate had a formal charge of −0.5, resulting in TS models with a charge of −5.0.

Molecular dynamics (MD) simulations of pol β-DNA-dTTP ternary complexes

Four Michaelis complexes, the MgMg structure with two Mg^{2+} ions (MgMg), the MgMg structure with two MD_6^{2+} molecules (MD_6MD_6), the MgNa structure with one Mg^{2+} and one Na^+ ion (MgNa), and the MgNa structure with one MD_6^{2+} molecule and one Na^+ ion (MD_6Na), were relaxed for 11 ps at 30 K. The resulting structures were then simulated at 100 K, 200 K, and 300 K for 1 ns, during which snapshots were collected every 5 ps for subsequent analysis. All simulations were carried out with the ENZYMIX module of MOLARIS,[23] using a very small positional restraint of 0.03 kcal/(mol*Å2) for all atoms within the explicitly treated simulation sphere of 20 Å radius. The two structures MgNa->MgMg and MgNa->MD_6MD_6 were relaxed for 11 ps at 30 K, simulated for 1.1 ns at 300 K, and analyzed at the end of the simulations.

All-atom LRA simulations of Michaelis and TS complexes

Several point mutants of pol β were prepared, focusing on mutations of charged residues to alanine in proximity to the nascent base pair (Figure 1A). For the wild type (WT) and the mutants R149A, R183A, and K280A of rat pol β, pre-steady state kinetic constants (k_{pol} and K_d) for the incorporation of nucleotides into single-nucleotide-gapped DNA molecules have been determined in the same experimental study[6] and are therefore assumed to be self-consistent. These pol β variants were used for the present study. Human and rat pol β share 96% sequence identity and none of the deviating amino acids are near the active site. Therefore, the studied mutations close to active site should have the same effects in rat and human pol β.[44] The incorporation of dCTP opposite template G (G:C) was studied for all variants and the incorporation of dTTP opposite template A (A:T) was studied for all variants except K280A, for which no experimental data are reported.[6] The equilibrium substrate binding constants (K_d) and the corresponding substrate binding free energies ΔG_{bind} as well as the catalytic efficiencies (k_{pol}/K_d) and the corresponding activation free energies $\Delta g^{\ddagger}_{enz}$ for these variants are summarized in Table 5. In an effort to reproduce these experimental data, the binding free energy of dNTP to the enzyme corresponding to ΔG_{bind} and the binding free energy of dNTP-TS to the enzyme corresponding to $\Delta g^{\ddagger}_{enz}$ were computed in a thermodynamic cycle employing the all-atom linear response approximation (LRA), as reported previously.[16] In that study, the all-atom LRA approach yielded significantly better agreement between experiment and computation than the much less expensive but less rigorous semimacroscopic protein dipole/Langevin dipole (PDLD/S) method in its LRA version (PDLD/S-LRA).[45] The latter is therefore not reported here. Mutations were introduced into the MgMg structure[9] by truncating the amino acid side chains to alanine side chains. Prior to these calculations, all systems were equilibrated for 101 ps at 30 K and for 100 ps at 310 K (the temperature at which the experiments were carried out[6]) using a positional restraint of 0.5 kcal/(mol*Å2) for all atoms in regions I and II. Region I contained the dNTP or dNTP-TS model, that is, the incoming dNTP plus the attacking O3′ of the primer. Region II contained all other atoms in the explicitly treated simulation sphere. This relatively small restraint mainly served to maintain correct base pairing

during the simulations. The all-atom LRA calculations were carried out over 5 ps on 30 automatically generated MD configurations for the uncharged and charged states using the POLARIS module of MOLARIS.[22] These configurations were collected over the course of 150 ps of simulation at 310 K.

Acknowledgements

This work was supported by NIH Grants 5U19CA105010, R01GM21422, the Center for High-Performance Computing and Communications (HPCC) at USC, and by the Intramural Research Program of the NIH, National Institute of Environmental Health Sciences.

References

1. Kornberg, A.; Baker, TA. DNA Replication. W. H. Freeman; New York: 1992.
2. Sancar A, Lindsey-Boltz LA, Unsal-Kacmaz K, Linn S. Molecular mechanisms of mammalian DNA repair and the DNA damage checkpoints. Annu Rev Biochem 2004;73:39–85. [PubMed: 15189136]
3. Rothwell PJ, Waksman G. Structure and mechanism of DNA polymerases. Adv Protein Chem 2005;71:401–40. [PubMed: 16230118]
4. Beard WA, Wilson SH. Structure and mechanism of DNA polymerase Beta. Chem Rev 2006;106:361–82. [PubMed: 16464010]
5. Wiebauer K, Jiricny J. Mismatch-specific thymine DNA glycosylase and DNA polymerase beta mediate the correction of G.T mispairs in nuclear extracts from human cells. Proc Natl Acad Sci U S A 1990;87:5842–5. [PubMed: 2116008]
6. Kraynov VS, Showalter AK, Liu J, Zhong XJ, Tsai MD. DNA polymerase beta: Contributions of template-positioning and dNTP triphosphate-binding residues to catalysis and fidelity. Biochemistry 2000;39:16008–16015. [PubMed: 11123928]
7. Sawaya MR, Pelletier H, Kumar A, Wilson SH, Kraut J. Crystal Structure of Rat DNA Polymerase β: Evidence for a Common Polymerase Mechanism. Science 1994;264:1930. [PubMed: 7516581]
8. Sawaya MR, Prasad R, Wilson SH, Kraut J, Pelletier H. Crystal structures of human DNA polymerase beta complexed with gapped and nicked DNA: evidence for an induced fit mechanism. Biochemistry 1997;36:11205–15. [PubMed: 9287163]
9. Batra VK, Beard WA, Shock DD, Krahn JM, Pedersen LC, Wilson SH. Magnesium-Induced Assembly of a Complete DNA Polymerase Catalytic Complex. Structure 2006;14:757–766. [PubMed: 16615916]
10. Fothergill M, Goodman MF, Petruska J, Warshel A. Structure-Energy Analysis of the Role of Metal Ions in Phosphodiester Bond Hydrolysis by DNA Polymerase I. J Am Chem Soc 1995;117:11619–11627.
11. Radhakrishnan R, Schlick T. Orchestration of cooperative events in DNA synthesis and repair mechanism unraveled by transition path sampling of DNA polymerase beta's closing. Proc Natl Acad Sci U S A 2004;101:5970–5975. [PubMed: 15069184]
12. Yang LJ, Beard WA, Wilson SH, Broyde S, Schlick T. Highly organized but pliant active site of DNA polymerase beta: Compensatory mechanisms in mutant enzymes revealed by dynamics simulations and energy analyses. Biophys J 2004;86:3392–3408. [PubMed: 15189842]
13. Florian J, Goodman MF, Warshel A. Computer simulation studies of the fidelity of DNA polymerases. Biopolymers 2003;68:286–299. [PubMed: 12601790]
14. Florian J, Goodman MF, Warshel A. Computer simulations of protein functions: Searching for the molecular origin of the replication fidelity of DNA polymerases. Proc Natl Acad Sci U S A 2005;102:6819–6824. [PubMed: 15863620]
15. Florian J, Goodman MF, Warshel A. Computer simulation of the chemical catalysis of DNA polymerases: Discriminating between alternative nucleotide insertion mechanisms for T7 DNA polymerase. J Am Chem Soc 2003;125:8163–8177. [PubMed: 12837086]
16. Xiang Y, Oelschlaeger P, Florian J, Goodman MF, Warshel A. Simulating the Effect of DNA Polymerase Mutations on Transition-State Energetics and Fidelity: Evaluating Amino Acid Group Contribution and Allosteric Coupling for Ionized Residues in Human Pol β. Biochemistry 2006;45:7036–7048. [PubMed: 16752894]

17. Shurki A, Warshel A. Structure/Function Correlations of Protreins using MM, QM/MM and Related Approaches; Methods, Concepts, Pitfalls and Current Progress. Adv Protein Chem 2003;66:249–312. [PubMed: 14631821]
18. Åqvist J. Ion-Water Interaction Potentials Derived from Free Energy Perturbation Simulations. J Chem Phys 1990;94:8021–8024.
19. Stote RH, Karplus M. Zinc binding in proteins and solution: a simple but accurate nonbonded representation. Proteins 1995;23:12–31. [PubMed: 8539245]
20. Hoops SC, Anderson KW, Merz KM. Force Field Design for Metalloproteins. J Am Chem Soc 1991;113:8262.
21. Cornell WD, Cieplak P, Bayly CI, Gould IR, Merz KM Jr, Ferguson DM, Spellmeyer DC, Fox T, Caldwell JW, Kollman PA. A Second Generation Force Field for the Simulation Of Proteins, Nucleic-Acids, And Organic-Molecules. J Am Chem Soc 1995;117:5179–5197.
22. Lee FS, Chu ZT, Warshel A. Microscopic and Semimicroscopic Calculations of Electrostatic Energies in Proteins by the POLARIS and ENZYMIX Programs. J Comput Chem 1993;14:161–185.
23. Chu, ZT.; Villa, J.; Strajbl, M.; Schutz, CN.; Shurki, A.; Warshel, A. MOLARIS version beta9.05. 2004.
24. Åqvist J, Warshel A. Free-Energy Relationships in Metalloenzyme-Catalyzed Reactions - Calculations of the Effects of Metal-Ion Substitutions in Staphylococcal Nuclease. J Am Chem Soc 1990;112:2860–2868.
25. Åqvist J, Warshel A. Computer Simulation of the Initial Proton Transfer Step in Human Carbonic Anhydrase I. J Mol Biol 1992;224:7–14. [PubMed: 1312606]
26. Pang YP, Xu K, Yazal JE, Prendergas FG. Successful molecular dynamics simulation of the zinc-bound farnesyltransferase using the cationic dummy atom approach. Protein Sci 2000;9:1857–65. [PubMed: 11106157]
27. Park JG, Sill PC, Makiyi EF, Garcia-Sosa AT, Millard CB, Schmidt JJ, Pang YP. Serotype-selective, small-molecule inhibitors of the zinc endopeptidase of botulinum neurotoxin serotype A. Bioorg Med Chem 2006;14:395–408. [PubMed: 16203152]
28. Pang YP. Successful molecular dynamics simulation of two zinc complexes bridged by a hydroxide in phosphotriesterase using the cationic dummy atom method. Proteins 2001;45:183–9. [PubMed: 11599021]
29. Oelschlaeger P, Schmid RD, Pleiss J. Insight into the mechanism of the IMP-1 metallo-beta-lactamase by molecular dynamics simulations. Protein Eng 2003;16:341–50. [PubMed: 12826725]
30. Oelschlaeger P, Schmid RD, Pleiss J. Modeling domino effects in enzymes: molecular basis of the substrate specificity of the bacterial metallo-beta-lactamases IMP-1 and IMP-6. Biochemistry 2003;42:8945–56. [PubMed: 12885227]
31. Kubo, R.; Toda, M.; Hashitsume, N. Statistical Physics II: Nonequilibrium Statistical Mechanics. Springer-Verlag; Berlin: 1985.
32. Hwang JK, Warshel A. Microscopic Examination of Free Energy Relationships for Electron Transfer in Polar Solvents. J Am Chem Soc 1987;109:715–720.
33. Schutz CN, Warshel A. What are the dielectric “constants” of proteins and how to validate electrostatic models. Proteins 2001;44:400–417. [PubMed: 11484218]
34. Arndt JW, Gong WM, Zhong XJ, Showalter AK, Liu J, Dunlap CA, Lin Z, Paxson C, Tsai MD, Chan MK. Insight into the catalytic mechanism of DNA polymerase beta: Structures of intermediate complexes. Biochemistry 2001;40:5368–5375. [PubMed: 11330999]
35. Noyes RM. Thermodynamics of ion hydration as a measure of effective dielectric properties of water. J Am Chem Soc 1962;84:513 – 522.
36. Pavlov M, Siegbahn PEM, Sandstrom M. Hydration of Beryllium, Magnesium, Calcium, and Zinc Ions Using Density Functional Theory. J Phys Chem A 1998;102:219–28.
37. Warshel A, Sussman F, King G. Free Energy of Charges in Solvated Proteins: Microscopic Calculations Using a Reversible Charging Process. Biochemistry 1986;25:8368–8372. [PubMed: 2435316]
38. Warshel, A. Computer Modeling of Chemical Reactions in Enzymes and Solutions. John Wiley & Sons; New York: 1991.

39. Frisch, MJ.; Trucks, GW.; Schlegel, BH.; Scuseria, GE.; Robb, MA.; Cheeseman, JR.; Montgomery, JA.; Kudin, KN.; Burant, JC.; Millam, JM.; Iyengar, SS.; Tomasi, J.; Barone, V.; Mennucci, B.; Cossi, M.; Scalmani, G.; Rega, N.; Petersson, GA.; Nakatsuji, H.; Hada, M.; Ehara, M.; Toyota, K.; Fukuda, R.; Hasegawa, J.; Ishida, M.; Nakajima, N.; Honda, Y.; Kitao, O.; Nakai, H.; Klene, M.; Li, X.; Knox, JE.; Hratchian, HP.; Cross, JB.; Adamo, C.; Jaramillo, J.; Gomperts, R.; Stratmann, RE.; Yazyev, O.; Austin, AJ.; Cammi, R.; Pomelli, C.; Ochterski, JW.; Ayala, PY.; Morokuma, K.; Voth, GA.; Salvador, P.; Dannenberg, JJ.; Zakrezewski, VG.; Dapprich, S.; Daniels, AD.; Strain, MC.; Farkas, O.; Malick, DK.; Rabuck, AD.; Raghavachari, K.; Foresman, JB.; Ortiz, JV.; Cui, Q.; Baboul, AG.; Clifford, S.; Cioslowski, J.; Stefanov, BB.; Liu, G.; Liashenko, A.; Piskorz, P.; Komaromi, I.; Martin, RL.; Fox, DJ.; Keith, T.; Al-Laham, MA.; Peng, CY.; Nanayakkara, A.; Challacombe, M.; Gill, PMW.; Johnson, B.; Chen, W.; Wong, MW.; Gonzalez, C.; Pople, JA. Gaussian03. 2003.

40. Miertus S, Scrocco E, Tomasi J. Electrostatic Interaction of a Solute with a Continuum. A Direct Utilization of Ab initio Molecular Potentials for the Prevision of Solvent Effects. J Chem Phys 1981;55:117–129.

41. Harding MM. Geometry of metal-ligand interactions in proteins. Acta Crystallogr D Biol Crystallogr 2001;57:401–11. [PubMed: 11223517]

42. King G, Warshel A. A Surface Constrained All-Atom Solvent Model for Effective Simulations of Polar Solutions. J Chem Phys 1989;91:3647–3661.

43. Jorgensen WL, Chandrasekhar J, Madura JD, Impey RW, Klein ML. Comparison of simple potential functions for simulating liquid water. J Chem Phys 1983;79:926 – 935.

44. Menge KL, Hostomsky Z, Nodes BR, Hudson GO, Rahmati S, Moomaw EW, Almassy RJ, Hostomska Z. Structure-function analysis of the mammalian DNA polymerase beta active site: Role of aspartic acid 256, arginine 254, and arginine 258 in nucleotidyl transfer. Biochemistry 1995;34:15934–15942. [PubMed: 8519750]

45. Lee FS, Chu ZT, Bolger MB, Warshel A. Calculations of Antibody-Antigen Interactions: Microscopic and Semi-Microscopic Evaluation of the Free Energies of Binding of Phosphorylcholine Analogs to McPC603. Protein Eng 1992;5:215–228. [PubMed: 1409541]

46. Humphrey W, Dalke A, Schulten K. VMD: visual molecular dynamics. J Mol Graph 1996;14:33–38. [PubMed: 8744570]

Abbreviations used

Pol β
: DNA polymerase β

MD
: molecular dynamics

LRA
: linear response approximation

PDLD/S
: semimacroscopic protein dipole/Langevin dipole

TS
: transition state

dNTP
: deoxynucleoside triphosphate

WT
: wild type

FEP
: free energy perturbation

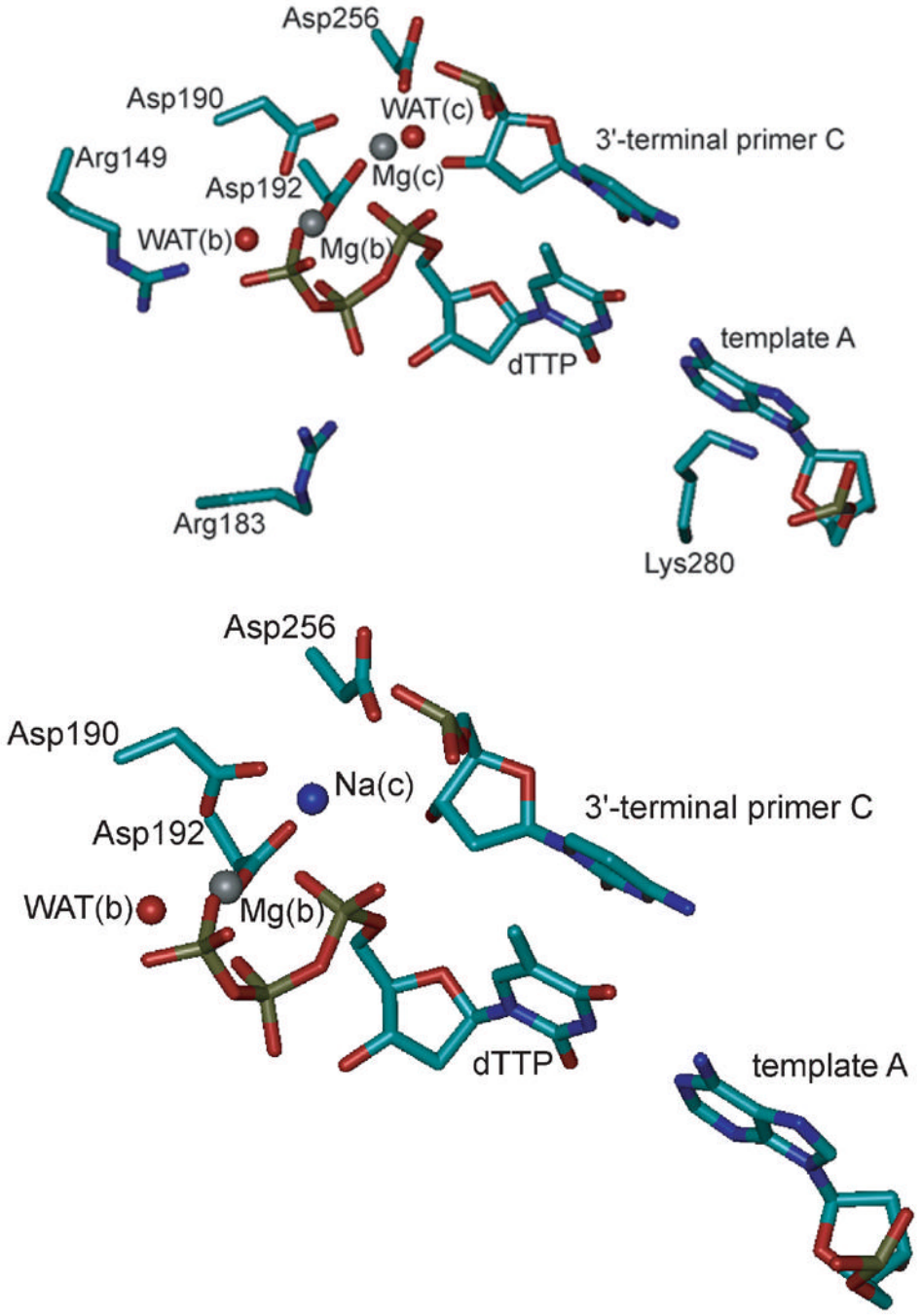

Figure 1.

Representation of the active sites of (A) the MgMg structure and (B) the MgNa structure used for MD simulations. The imido nitrogen bridging the α- and β-phosphate groups of the dUTP analogue in the crystal structures was mutated to a phosphodiester oxygen and the uracil part was mutated to thymidine, thus generating dTTP. The side chains and Cα atoms of amino acids are shown as sticks, colored by atom (cyan, C; blue, N; red, O), and labeled at the Cα atom. Nucleotides are shown as sticks, colored by atom (copper, P), and labeled at the base. Oxygens of water molecules are shown as red spheres. Mg^{2+}ions are shown as grey spheres and the Na^{+} ion as a blue sphere. (A) The two Mg^{2+} ions Mg(b) and Mg(c) and their ligands are shown.

Both metal ions are coordinated octahedrally. In addition, the templating nucleotide (template A) and amino acids that were mutated in this study (Arg149, Arg183, and Lys280) are shown. (B) The Mg^{2+} ion Mg(b) and the Na^{+} ion Na(c) and their ligands are shown. While Mg(b) is coordinated octahedrally, Na(c) is coordinated in a distorted tetrahedral fashion with relatively large Na(c)-ligand distances (2.19–2.74 Å). Note that the water molecule coordinated to Mg (c) [WAT(c)] in the MgMg structure is missing in the MgNa structure and that O3′ of the primer C is not ligating Na(c) (3.54 Å) and is not positioned for nucleophilic attack on the dTTP αP (4.70 Å). The figures were generated with VMD,[46] version 1.8.3.

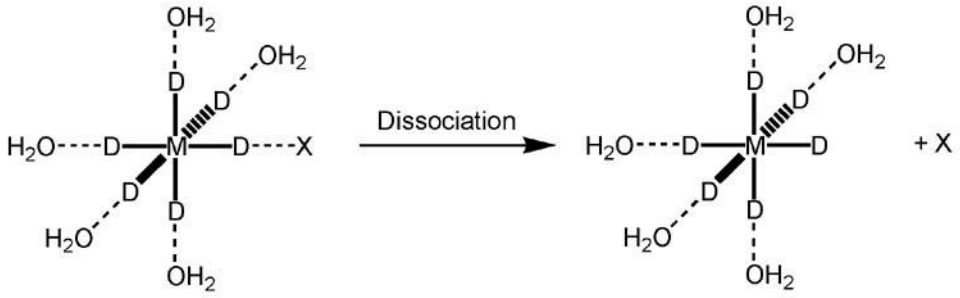

Figure 2.

Scheme of the model complexes used for the calculations presented in Tables III and IV. The measured distances are the distances between the central atom M and the ligand X of interest in the intact complex shown on the left. Dissociation energies were calculated as the difference between the energy of the intact complex $[MD_6(H_2O)_5]^{2+}X$ (left side) and the sum of the energies of the fragments $[MD_6(H_2O)_5]^{2+}$ and X resulting from dissociation (right side). For DFT calculations, the MD_6^{2+} molecule was replaced by a Mg^{2+} atom.

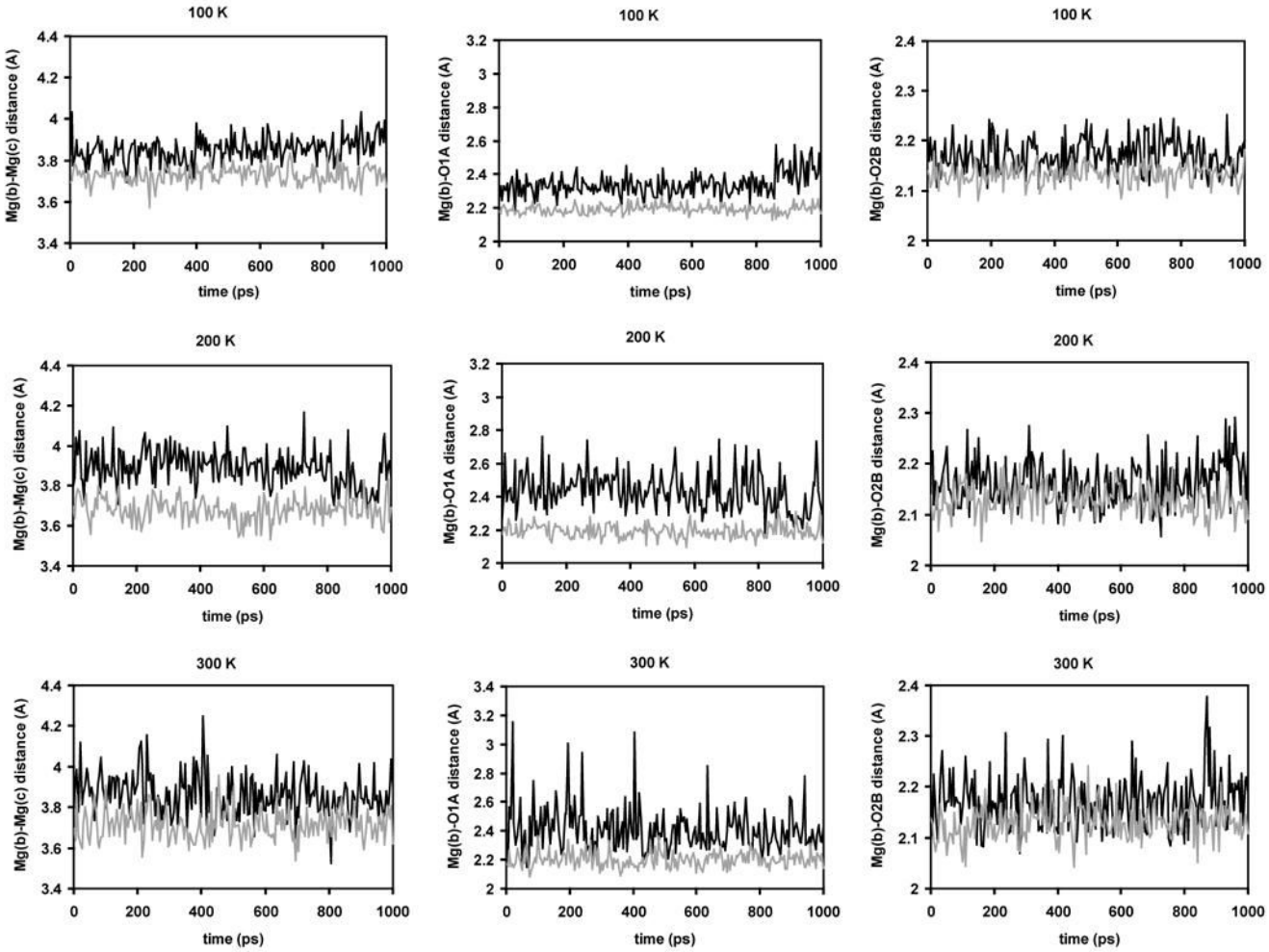

Figure 3.

Critical distances in the active site of the MgMg structure over the course of 1 ns MD simulations at different simulation temperatures (panels A, B, and C: 100 K; panels D, E, and F: 200 K; panels G, H, and I: 300 K) using the regular Mg^{2+} model (black) and the MD_6^{2+} model (grey). Panels A, D, and G show the Mg(b)-Mg(c) distance; panels B, E, and H the Mg (b)-O1A distance; and panels C, F, and I the Mg(b)-O2A distance.

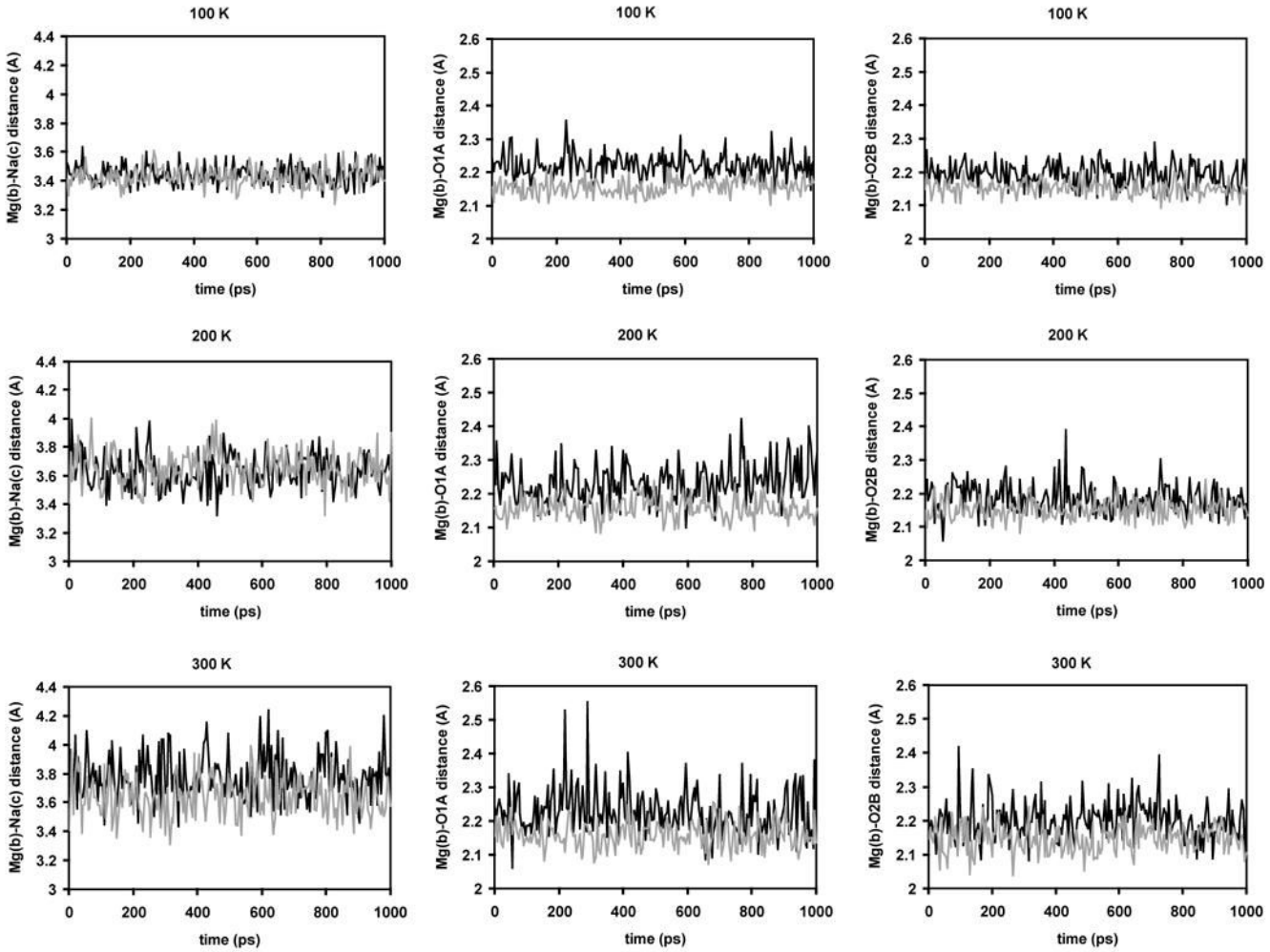

Figure 4.

Critical distances in the active site of the MgNa structure over the course of 1 ns MD simulations at different simulation temperatures (panels A, B, and C: 100 K; panels D, E, and F: 200 K; panels G, H, and I: 300 K) using the regular Mg^{2+} model (black) and the MD_6^{2+} model (grey). Panels A, D, and G show the Mg(b)-Na(c) distance; panels B, E, and H the Mg(b)-O1A distance; and panels C, F, and I the Mg(b)-O2A distance.

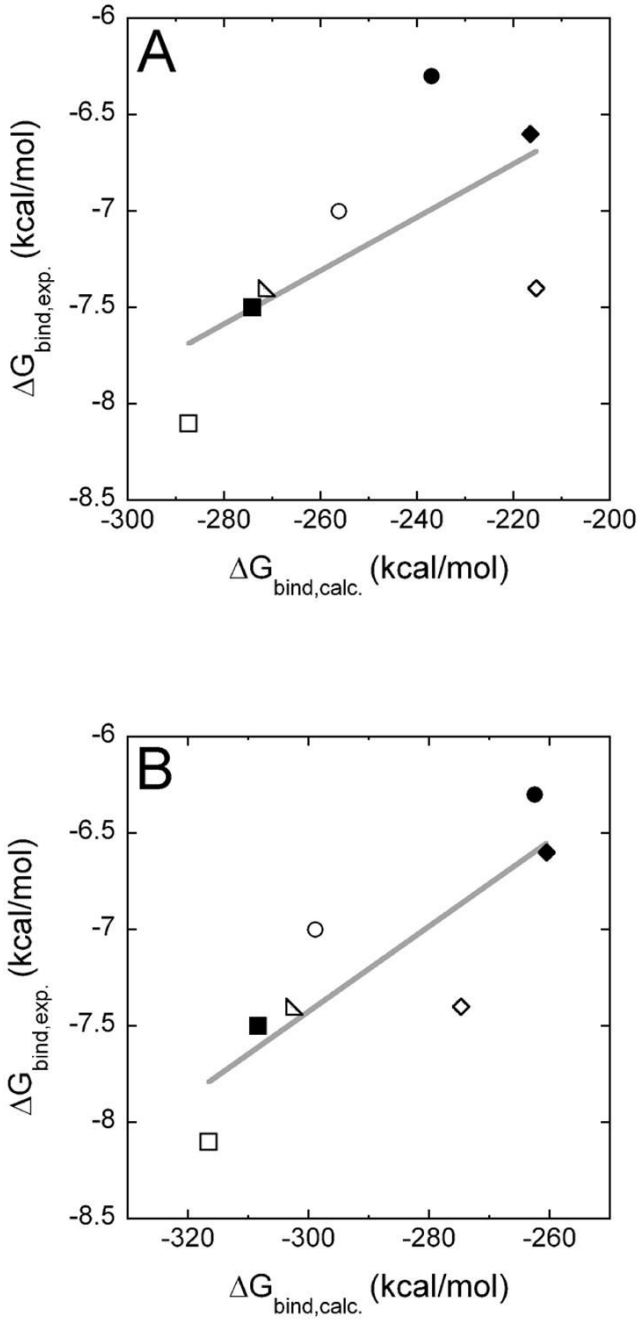

Figure 5.

The experimentally determined pre-steady-state substrate binding energies $\Delta G_{bind,\ exp}$. are plotted versus the calculated substrate binding free energies $\Delta G_{bind,\ calc}$., which were obtained using the regular Mg^{2+} model (panel A) or the MD_6^{2+} model (panel B). The following pol β variants/nascent base pairs (template base:incorporated base) are shown: ■ WT/A:T; ● R149A/A:T; ◆ R183A/A:T; □WT/G:C; ○ R149A/G:C; ◇ R183A/G:C; △ K280A/G:C.

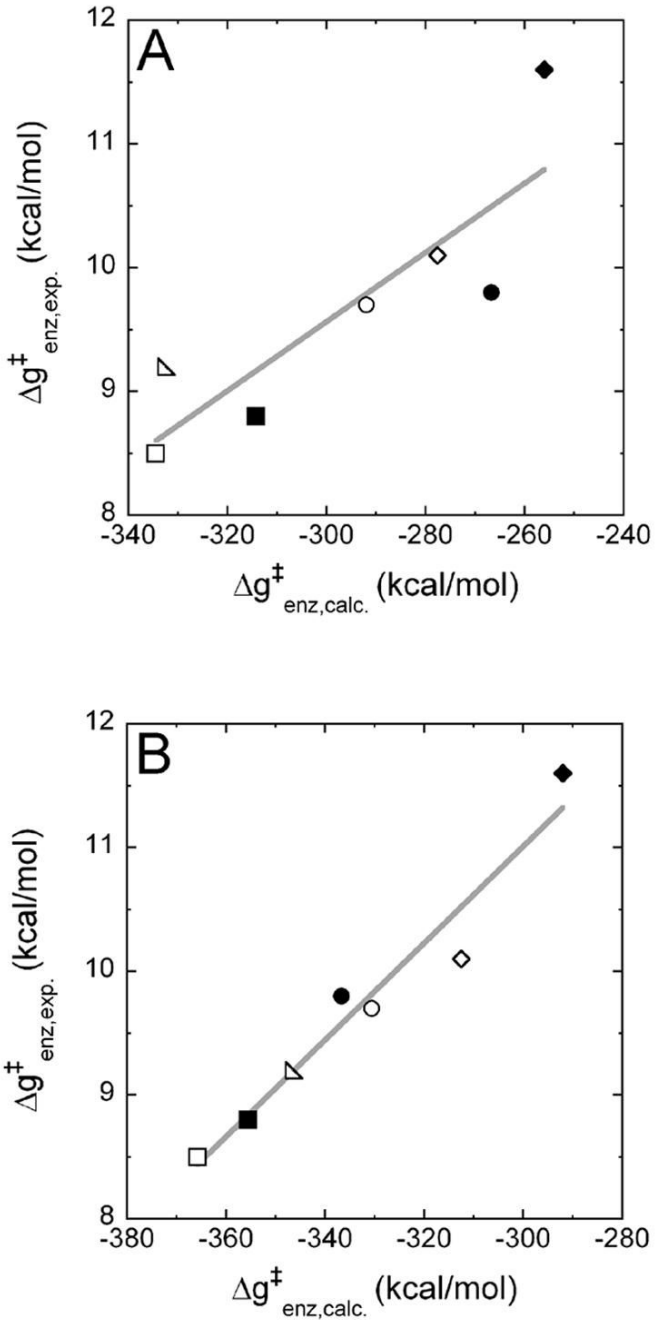

Figure 6.

The experimentally determined equilibrium TS binding energies $\Delta g^{\ddagger}_{enz,\,exp.}$ are plotted versus the calculated TS binding free energies $\Delta g^{\ddagger}_{enz,\,calc.}$, which were obtained using the regular Mg^{2+} model (panel A) or the MD_6^{2+} model (panel B). The following pol β variants/nascent base pairs (template base:incorporated base) are shown: ■ wild type (WT)/A:T; ● R149A/A:T; ♦ R183A/A:T; □ WT/G:C; ○ R149A/G:C; ◊R183A/G:C; △ K280A/G:C.

Table 1

Force field parameters for MD_6^{2+} molecules

Bond			***K*** **[kcal/(mol*Å^2)]**	r_0 **(Å)**
M-D_i[a]			640	0.900
D_i-$D_{j \neq i}$			640	1.273
Angle			K [kcal/(mol*rad^2)]	θ_0 (deg.)
D_i-M-D_i			55	180
D_i-M-$D_{j \neq i}$			55	90
M-D_i-$D_{j \neq i}$			55	45
D_i-$D_{j \neq i}$-D_i			55	90
D_i-$D_{j \neq i}$-$D_{k \neq j \neq i}$			55	60
Atom	Mass	Charge	A_{vdW}[b]	B_{vdW}[c]
M	6.3	−1.0	70.00	41.00
D	3.0	+0.5	0.05	0.00

[a] To distinguish positions, dummy atoms at opposite corners of the octahedral molecule are called D_i, whereas those adjacent to D_i are called $D_{j \neq i}$ and $D_{k \neq j \neq k}$.

[b] $A_{vdW} = [\varepsilon (2R^*)^{12}]^{1/2}$

[c] $B_{vdW} = [2\varepsilon (2R^*)^6]^{1/2}$

Table 2

Comparison of solvation free energies of MD_6^{2+} with ab initio and experimental data.[†]

	AC-FEP using the ENZYMIX force field[a]			
	reg.[b]	pol.[c]	DFT[d]	Experiment[e]
Solvation free energy (kcal/mol)	−456.3	−456.2	−460.8	−454.2

[†]The solvation free energies of MD_6^{2+} were calculated with an adiabatic charging-free energy perturbation (AC-FEP) approach using the ENZYMIX module of the MOLARIS program. The corresponding values obtained for Mg^{2+} in DFT calculations and in experiment are given for comparison.

[a]For these calculations, MD_6^{2+} was immersed in a surface-constrained[42] 20 Å radius sphere of TIP3P[43] water molecules, a 22 Å radius sphere of Langevin dipoles, and a surrounding continuum solvent model.[22]

[b]reg. designates that the regular, nonpolarizable ENZYMIX force field was used.

[c]pol. designates that the polarizable ENZYMIX force field was used.

[d]This value is taken from Pavlov et al.[36] In that study, $[Mg(H_2O)_6](H_2O)_{12}^{2+}$ was minimized and then the energy was calculated at the B3LYP/6-311 +G** level.

[e]This value is taken from Noyes (1962).[35]

Table 3

Comparison of calculated distances and dissociation energies in $[MD_6(H_2O)_5]^{2+}X$ complexes in the gas phase with ab initio calculations.[†]

	distance (Å)				dissociation energy (kcal/mol)[a]			
	ENZYMIX				ENZYMIX			
Ligand X	reg.[b]	pol.[c]	AMBER	DFT	reg.[b]	pol.[c]	AMBER	DFT
H_2O	2.06	2.10	2.09	2.15	41	42	47	34
CH_3OH	2.10	2.11	2.09	2.09	37	43	48	43
PO_3^-	2.02	2.06	2.15	1.94	237	246	221	200
HPO_4^{2-}	1.97	1.97	2.16	1.91	446	418	434	348

[†]The model complexes used are shown schematically in Figure 2. These complexes were minimized using the ENZYMIX or AMBER force field. The force field parameters of MD_6^{2+} (Table I) were fit to reproduce the corresponding values of $[Mg(H_2O)_5]^{2+}X$ obtained from DFT calculations at the B3LYP/6-311++G** level.

[a]The energy required to remove the ligand X from the complex (see Figure 2).

[b]reg. designates that the regular, nonpolarizable ENZYMIX force field was used.

[c]pol. designates that the polarizable ENZYMIX force field was used

Table 4

Comparison of calculated distances in $[MD_6(H_2O)_5]^{2+}X$ complexes in solution with experimental data.[†]

	distance (Å)			
	ENZYMIX			
Ligand X	reg.[a]	pol.[b]	AMBER	Experiment
H_2O	2.05	2.07	2.09	2.07[c]
CH_3OH	2.09	2.09	2.08	2.19[c]
PO_3^-	2.02	2.07	2.14	2.03–2.19[d]
HPO_4^{2-}	2.02	2.04	2.07	

[†] For these calculations, the complexes were immersed in a surface-constrained[42] 20 Å radius sphere of TIP3P[43] water molecules, a 22 Å radius sphere of Langevin dipoles, and a surrounding continuum solvent model.[22] For comparison, the corresponding distances in X-ray crystal structures are given.

[a] reg. designates that the regular, nonpolarizable ENZYMIX force field was used.

[b] pol. designates that the polarizable ENZYMIX force field was used.

[c] These values are taken from Harding;[41] the ligands in protein X-ray crystal structures corresponding to methanol are serine and threonine.

[d] These values are taken from the pol β structures recently published by Batra et al.;[9] the ligands in the X-ray crystal structure corresponding to PO_3^- and HPO_4^{2-} are different magnesium-coordinating, nonbridging triphosphate oxygens.

Table 5A

Critical distances in simulations of the MgMg structure

Temperature (K)	Structure/ Model	Mg(b)-Mg (c) distance (Å)	Mg(b)-O1A distance (Å)	Mg(b)-O2B distance (Å)
	Crystal structure[9]	3.43	2.06	2.04
100	MgMg	3.85 ± 0.06	2.34 ± 0.06	2.17 ± 0.03
	MD_6MD_6	3.73 ± 0.04	2.19 ± 0.03	2.13 ± 0.02
200	MgMg	3.89 ± 0.09	2.43 ± 0.12	2.16 ± 0.04
	MD_6MD_6	3.68 ± 0.06	2.19 ± 0.04	2.13 ± 0.03
300	MgMg	3.86 ± 0.10	2.41 ± 0.15	2.17 ± 0.05
	MD_6MD_6	3.71 ± 0.07	2.20 ± 0.05	2.13 ± 0.03

Table 5B

Critical distances in simulations of the MgNa structure

Temperature (K)	Structure/ Model	Mg(b)-Na (c) distance (Å)	Mg(b)-O1A distance (Å)	Mg(b)-O2B distance (Å)
	Crystal structure[9]	3.40	2.05	2.03
100	MgNa	3.45 ± 0.06	2.22 ± 0.04	2.20 ± 0.03
	MD_6Na	3.43 ± 0.06	2.15 ± 0.02	2.15 ± 0.02
200	MgNa	3.62 ± 0.13	2.22 ± 0.05	2.19 ± 0.05
	MD_6Na	3.66 ± 0.12	2.16 ± 0.03	2.15 ± 0.03
300	MgNa	3.78 ± 0.16	2.24 ± 0.07	2.20 ± 0.06
	MD_6Na	3.63 ± 0.14	2.16 ± 0.04	2.14 ± 0.04

Table 6A

Dissociation constants for dNTP (K_d) determined in pre-steady state experiments for the incorporation of T opposite A (A:T) and C opposite G (G:C) for several pol β variants.[6]

	A:T		G:C	
Pol β variant	**K_d (μM)**	**ΔG_{bind} (kcal/mol)**	**K_d (μM)**	**ΔG_{bind} (kcal/mol)**
WT	5.4	−7.5	1.9	−8.1
R149A	35	−6.3	12	−7.0
R183A	21	−6.6	5.9	−7.4
K280A	n.a.[a]	n.a.[a]	6	−7.4

Table 6B

Catalytic efficiencies (k_{pol}/K_d) determined in pre-steady state experiments for the incorporation of T opposite A (A:T) and C opposite G (G:C) for several pol β variants.[6]

Pol β variant	A:T		G:C	
	k_{pol}/K_d ($s^{-1}M^{-1}$)	$\Delta g^{\ddagger}_{enz}$ (kcal/mol)	k_{pol}/K_d ($s^{-1}M^{-1}$)	$\Delta g^{\ddagger}_{enz}$ (kcal/mol)
WT	4,100,000	8.8	6,600,000	8.5
R149A	685,000	9.8	920,000	9.7
R183A	43,000	11.6	440,000	10.1
K280A	n.a.[a]	n.a.[a]	2,000,000	9.2

[a] n.a., not available.